


Article

Effect of Graphene Oxide Modified with Organic Amine on the Aging Resistance, Rolling Loss and Wet-Skid Resistance of Solution Polymerized Styrene-Butadiene Rubber

Songhan Wan ¹, Xiaobin Lu ¹, Hongguo Zhao ², Songbo Chen ¹, Shuwei Cai ¹, Xianru He ^{1,*}  and Rui Zhang ³

¹ School of Materials Science and Engineering, Southwest Petroleum University, Chengdu 610500, China; songhanwan@foxmail.com (S.W.); xblu1009@163.com (X.L.); chen756424838@foxmail.com (S.C.); victor8951@foxmail.com (S.C.)

² Petrochemical Research Institute, PetroChina, Lanzhou 730060, China; zhaohongguo@petrochina.com.cn

³ Institute für Physik, Universität Rostock, 18051 Rostock, Germany; rui.zhang@uni-rostock.de

* Correspondence: xrhe@swpu.edu.cn

Received: 4 February 2020; Accepted: 21 February 2020; Published: 25 February 2020



Abstract: Graphene oxide (GO) was modified by p-phenylenediamine (PPD), aiming at improving the wet-skid resistance and reduce the rolling loss of solution polymerized styrene-butadiene rubber (SSBR). PPD with amino groups enabled GO to obtain anti-aging function. The structure of modified GO (PPD-GO) was characterized by Fourier transform infrared spectroscopy (FTIR), X-ray diffraction (XRD) and Raman spectroscopy. Mechanical tests showed that the mechanical properties of SSBR before and after aging were improved by adding PPD-GO. The results of thermogravimetric-differential scanning calorimeter synchronization analysis (TGA-DSC) indicated that SSBR/PPD-GO obtained good thermo-oxidative stability. The dynamic mechanical analysis (DMA) of SSBR composites showed that the mechanical loss factor ($\tan\delta$) peak moved to high temperature with the content of PPD-GO. The $\tan\delta$ values of SSBR composites showed that it had a good effect on improving the wet-skid resistance and reducing the rolling loss of SSBR by adjusting the content of PPD-GO. In particular, with the addition of 4 phr GO, SSBR was effectively improved in mechanical properties, aging resistance, wet-skid resistance and low rolling loss.

Keywords: p-phenylenediamine (PPD); graphene oxide (GO); solution polymerized styrene-butadiene rubber (SSBR); aging resistance; rolling loss; wet-skid resistance

1. Introduction

Solution polymerized styrene-butadiene rubber (SSBR), with good elasticity, abrasion resistance, low rolling loss and wet-skid resistance, is widely used in the field of tread adhesive [1,2]. With the continuous development of the tire industry, higher requirements are put forward for the comprehensive performance of tread adhesive. The unsaturated double bonds make it easy for the aging resistance of SSBR to be decreased in the thermal-oxidative environment [3,4]. Therefore, it is necessary to improve the aging resistance while reducing the rolling loss and improving the wet-skid resistance of SSBR.

In the past decades, nanoparticles have received increasing interest owing to its unique structural and surface properties. There are many nanoparticles have been applied to improve the performances of rubber, such as graphene [5–8], layered double hydroxide [9,10], nano silica [11], carbon nano tubes [12], montmorillonite [13,14], ect. The properties of nanocomposites are better than that of conventional composites in the same composition due to the quantum effect and surface effect caused by the small

size and large specific surface area. Graphene is a kind of two-dimensional carbon nanoparticle with high mechanical strength, excellent thermal and electrical conductivities [15–17]. According to researches, graphene allows rubber to achieve better overall performances. Yingyan Mao [18] prepared GO/silica/styrene-butadiene rubber composites. The wet-skid resistance of the composites increased, and the rolling loss decreased by about 10% when GO was added with a volume fraction of 0.6%. Chengpeng Li [19] modified natural rubber with graphene and found that the tensile strength of natural rubber increased by 9% when the addition of graphene accounted for only 0.07% of the volume fraction. S.H. Song [20] found that the thermal conductivity of styrene-butadiene rubber composites increased by about 20% when the addition amount of graphene was only 5% of the mass fraction, which far exceeding that of carbon black and other fillers of the same amount.

Graphene is easy to agglomerate in the polymer matrix due to the large specific surface and strong interaction between layers [21]. Therefore, many researches paid attention to modify graphene to improve its dispersibility in the polymer matrix. Graphene oxide (GO) is the derivative of graphene, with plenty of oxygen-containing groups, such as hydroxyl, epoxy group and carboxyl groups, which offers potential for the preparation of modified graphene [16,17]. Therefore, chemical grafting is an effective method to obtain modified GO [22–26]. For example, it was reported that alkylamine was covalently grafted to GO. The dispersion of GO in the rubber matrix was significantly improved [27].

Diamine grafted onto GO is an effective way to improve the thermostability and anti-aging property of polymers [6,28,29]. Junjun Zhou et al. found that the thermal oxidation resistance of SBR was effectively promoted by graphene oxide (GO) functionalized with the 4-aminodiphenylamine [30]. Zhong used an efficient one-step approach, which was developed to simultaneously reduce and functionalize GO via N-1, 3-dimethylbutyl-N'-phenyl-p-phenylenediamine. It was found that the SBR adding with the functionalized graphene exhibited high long-term thermo-oxidative aging resistance [31]. P-phenylenediamine (PPD), with the anti-aging amino groups, is not only beneficial to improve the interaction between GO and SSBR matrix, but also can endow GO with anti-aging function [32,33]. Many researches devoted to enhancement of polymers properties by modified graphene oxide, but most of them only looked at one aspect of performance improvement, such as mechanical properties, thermal stability, and so on.

In the present study, GO was grafted by PPD to obtain the functionalized particle, PPD-GO. PPD-GO was added into SSBR, aiming at improving the wet-skid resistance and reducing rolling loss while improving the aging resistance of SSBR.

2. Materials and Methods

2.1. Materials

The SSBR with styrene content 25.7% was obtained from China National Petroleum Corporation (CNPC) Lanzhou Petrochemical Company (Lanzhou, China). Graphite oxide was supplied by the Sixth Element Materials Technology co, LTD. (Changzhou, China). Zinc oxide (ZnO), sulfur, stearic acid, $\text{NH}_3\cdot\text{H}_2\text{O}$ and absolute ethyl alcohol were supplied by Chengdu Kelong Chemical Reagent co. LTD (Chengdu, China). P-phenylenediamine (PPD) was purchased from China Aladdin Industrial Corporation (Shanghai, China). Carbon black was obtained from Hongying carbon black factory (Chengdu, China). N-tert-butyl-2-benzothiazole sulfonamide (TBBS) was purchased from Duba new material technology co. LTD (Dongguan, China).

2.2. The Synthesis of PPD-GO

GO was obtained by mechanical ultrasonic stripping of graphite oxide. 1 g of graphite oxide was added into 1000 mL deionized water for ultrasonic dispersion (Huashen science and technology equipment co. LTD; Shen Zhen, China), with time of 2 h and the ultrasonic frequency was 3.5 kHz. The ultrasound products were freeze-dried to obtain the GO. The pH of 1000 mL deionized water was adjusted to about 10 by dropping $\text{NH}_3\cdot\text{H}_2\text{O}$. Then 1 g of GO and 2 g of PPD were added for reaction

at a temperature of 80 °C and a time of 12 h. Finally, the reaction products were filtered, rinsed and freeze-dried to obtain the PPD-GO particles. The Schematic diagram of the synthesis of PPD-GO was showed in Figure 1.

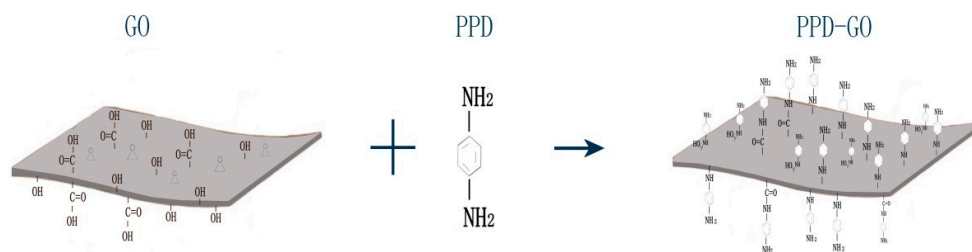


Figure 1. The Schematic diagram of the synthesis of p-phenylenediamine–graphene oxide (PPD-GO).

2.3. The Preparation of SSBR Composite

SSBR, particles and additives were mixed in a two-roll mixing mill (Guangdong Zhanjiang Rubber and Plastic Machinery Factory, Zhanjiang, China). The compositions of the SSBR composites were shown in the Table 1. The vulcanizing of the mixed rubber was carried out with the flat vulcanizer (Shanghai Rubber Machinery Factory, Shanghai, China) under a pressure 10 MPa at 145 °C for 35 min.

Table 1. The list of experimental formula (parts per hundreds of rubber).

Sample	SSBR	ZnO	Stearic Acid	Sulfur	TBBS	Carbon Black	PPD-GO
SSBR	100	2.18	0.73	1.27	1.00	50.00	0
PPD-GO1	100	2.18	0.73	1.27	1.00	50.00	1.00
PPD-GO2	100	2.18	0.73	1.27	1.00	50.00	2.00
PPD-GO3	100	2.18	0.73	1.27	1.00	50.00	3.00
PPD-GO4	100	2.18	0.73	1.27	1.00	50.00	4.00
PPD-GO5	100	2.18	0.73	1.27	1.00	50.00	5.00

2.4. Characterization

Fourier transform infrared spectra (FTIR) analysis was carried out by the Thermo Fisher Scientific Nicolet iS50 infrared spectrometer (Waltham, MA, USA) with the scanning speed of 4 cm⁻¹/min from 500 cm⁻¹ to 4000 cm⁻¹. KBr pellets were used in the test.

X-ray diffraction (XRD) diffractograms were obtained using a PANalytical B.V. X Pert PRO MPD X-ray diffractometer (PANalytical, Almelo, The Netherlands), equipped with Cu K α radiation ($\lambda = 0.154$ nm). The scanning diffraction angle was from 3° to 70° with a scanning rate of 4°/min.

Raman analysis was characterized by the spectrometer of ID Raman micro IM-52AV300 (Weihai Optical Instrument). The excitation source was He-Ne laser with a wavelength of 785 nm and a scanning range of 200 ~ 2000 cm⁻¹.

Scanning electron microscopy (SEM) analysis was performed on a JSM-6360LV instrument (Japan Electronics Co, Tokyo, Japan) to study the fracture surface morphology of SSBR composites.

Tensile test was conducted on a MTS CMT 6104 universal tensile testing machine (MTS Systems (China) Co., Ltd., Shanghai, China) according to the standard of GB/ t528-2009. The samples were cut into a dumbbell shape with thickness of 2 mm, width of 6 mm and the middle standard length of 25 mm.

Thermogravimetric-differential scanning calorimeter synchronization analysis (TGA-DSC) was carried out on a NETZSCH STA449F3 Jupiter instrument (NETZSCH, Bavaria, Germany) with the heating rate of 10 °C/min from 40 °C to 800 °C. The measurements were done under oxygen atmosphere with a gas flow rate of 20 mL/min.

Dynamic mechanical analysis (DMA) was carried out on a TA Q800 apparatus (TA Instruments, New Castle, DE, USA) with heating rate of 3 °C/min from −80 °C to 60 °C. The amplitude was 15 μm, and the frequency was 1 Hz. The size of the sample was 60 mm long, 12.8 mm wide and 2 mm thick.

3. Results and Discussion

3.1. The Characterization of Structure of PPD-GO

The PPD-GO was confirmed by FTIR spectroscopy. As shown in Figure 2 and Table 2, the curve of GO showed two peaks at 3423 cm^{−1} and 1404 cm^{−1}, which corresponding to the hydroxyl and carboxyl, respectively. The peaks at 1721 cm^{−1}, 1620 cm^{−1} and 1048 cm^{−1} were attributed to C=O in carboxyl group, C=C and C–O–C in epoxide group. In the curve of PPD, the appearance of two peaks at about 3417 cm^{−1} were assigned to the stretching vibration of –N–H of NH₂. The peaks at 1623 cm^{−1} and 1520 cm^{−1} were attributed to the bending vibration of N–H of NH₂. Compared with the curves of PPD and GO, there were two new peaks at 1173 cm^{−1} and 727 cm^{−1} appeared on the curve of PPD-GO, which corresponding the stretching vibration of C–N and the stretching vibration of N–H of C–NH–, respectively [34,35]. Meanwhile, the peak at 3210 cm^{−1} was attributed to the H-bond interaction between –NH₂ and oxygen-containing groups of GO [28]. It indicated the formation of C–NH–C bands due to the grafting of PPD to GO surface.

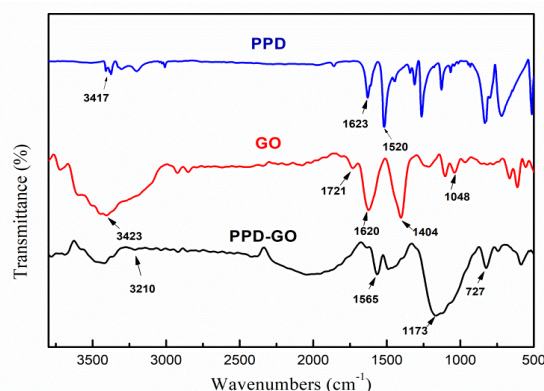


Figure 2. Fourier transform infrared (FTIR) spectra of PPD, GO and PPD-GO.

Table 2. The FTIR bands assignments.

GO		PPD		PPD-GO	
Wavenumber(cm ^{−1})	Group	Wavenumber(cm ^{−1})	Group	Wavenumber(cm ^{−1})	Group
3423	–OH	3417	–NH	3210	H-bond
1721	C=O	1623, 1520	N–H of NH ₂	1173	C–N
1620	C=C	-	-	727	N–H of C–NH–
1404	–COOH	-	-	-	-
1048	C–O–C	-	-	-	-

In X-ray diffractograms (Figure 3), there was only one peak on the spectra of GO at 11.06°, corresponding the crystal face (002). After PPD was grafted onto GO, the crystal face (002) transferred to 6.55° and the basal spacing (002) increased from 0.85 nm to 1.35 nm, indicating that a certain amount of PPD entered the interlayer of GO. It was noting that there was a broad peak on the spectra of PPD-GO at 24.98°, which coincided with the characteristic peak of graphene, indicating that PPD had a reduction effect on GO. In the curve of PPD-G, there were many small peaks between the 2θ of about 15°–30°, indicated that GO was exfoliated to some extent and PPD formed small polymeric crystallites on the GO sheets [36].

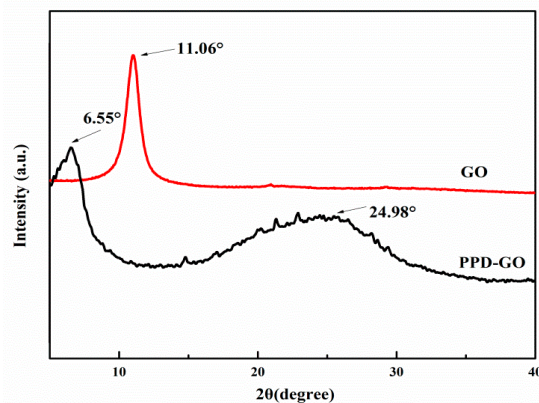


Figure 3. X-ray diffractograms of the GO and PPD-GO.

The intensity ratio (I_D/I_G) of the D-peak to G-peak of the Raman spectra of graphene is commonly used to characterize the defect density of graphene [37–40]. In the Raman spectra of GO and PPD-GO (Figure 4), D peak and G peak appeared around 1310 cm^{-1} and 1580 cm^{-1} respectively. The I_D/I_G of PPD-GO was 1.49, which was 0.24 higher than that of GO. This is because the amino group of PPD reacted with the oxygen-containing group on GO, resulting in the decrease of the average size of the sp^2 domain [30].

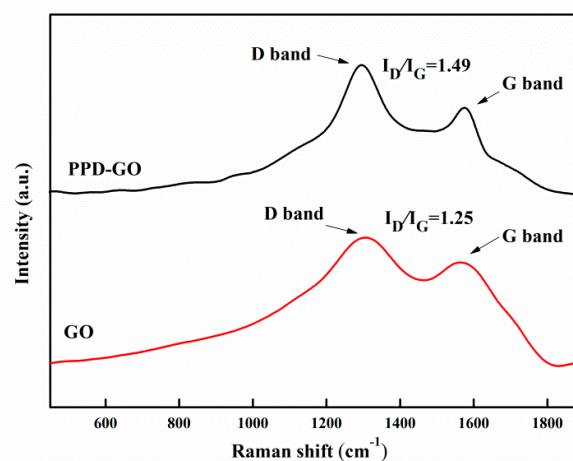


Figure 4. Raman spectra of GO and PPD-GO.

3.2. The Mechanical Properties of SSBR Composites Before and After Aging.

Tensile tests were conducted to evaluate the mechanical properties of SSBR composites. It can be seen from Figure 5a and Table 3 that SSBR/PPD-GO composites had better mechanical properties than SSBR without PPD. In particular, the tensile strength and the elongation at break of SSBR/PPD-GO4 were 21.5 MPa and 350%, respectively. When the amount of PPD-GO reached 5 phr, the mechanical properties of SSBR/PPD-GO decreased to the values comparable to those for SSBR. This is due to the fact that PPD-GO agglomerated in the SSBR matrix when the amount of PPD-GO increased, resulting in a decrease in mechanical properties. In order to investigate the effect of PPD-GO on the thermo-oxidative aging resistance, SSBR composites were selected to conduct the thermal-oxygen aging test at $90\text{ }^\circ\text{C}$ for 96 h. After thermal oxygen aging, mechanical properties of rubber will change significantly. In Figure 5b and Table 3, the elongation at break of SSBR/PPD-GO composites was almost equivalent to that of SSBR, which showed a slight trend of increasing first and decreasing later. The tensile strength of SSBR/PPD-GO composites was about 1.3 MPa higher. It was indicated that

PPD-GO can not only significantly improve the mechanical properties of SSBR, but also effectively enhance the aging resistance of SSBR.

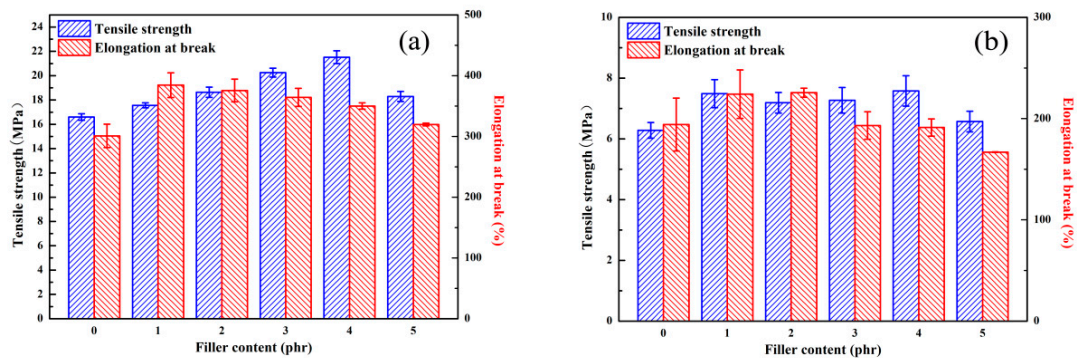


Figure 5. Tensile strength and elongation at break of solution polymerized styrene-butadiene rubber (SSBR) composites with different PPD-GO content before aging (a) and after aging (b).

Table 3. Mechanical properties SSBR composites before and after aging.

Sample		SSBR	PPD-GO1	PPD-GO2	PPD-GO3	PPD-GO4	PPD-GO5
tensile strength (Mpa)	before aging	16.6 ± 0.3	17.6 ± 0.2	18.6 ± 0.4	20.3 ± 0.4	21.5 ± 0.5	18.3 ± 0.4
	after aging	6.3 ± 0.3	7.5 ± 0.5	7.9 ± 0.3	7.3 ± 0.4	7.6 ± 0.5	6.6 ± 0.3
elongation at break (%)	before aging	301 ± 19	384 ± 20	375 ± 18	364 ± 14	350 ± 5	319 ± 2
	after aging	194 ± 26	224 ± 23	225 ± 4	193 ± 13	181 ± 8	166 ± 2

3.3. The Thermal Properties of SSBR Composites

The synchronous thermal analysis of SSBR composites was tested under oxygen atmosphere. The content of PPD-GO was 4 phr. In Figure 6a, the TGA curve of SSBR composites was mainly divided into two stages. The first stage was from 200 °C to 440 °C, which mainly attributed to the primary degradation of rubber chains. The second stage was from 440 °C to 600 °C, which attributed to the further degradation of rubber and thermal oxidation degradation of carbon black. In the first stage, the temperature corresponding to the maximum degradation rate of SSBR/PPD-GO was 10 °C higher than that of SSBR. This is because some of the free radicals generated in the thermal oxygen degradation process were captured by the amino group on PPD-GO [6]. Figure 6b showed the DSC curve of SSBR/PPD-GO. The exothermic peak of SSBR in the whole degradation process was more obvious than that of SSBR/PPD-GO, indicating that the PPD-GO effectively slowed down the thermal oxygen degradation of SSBR.

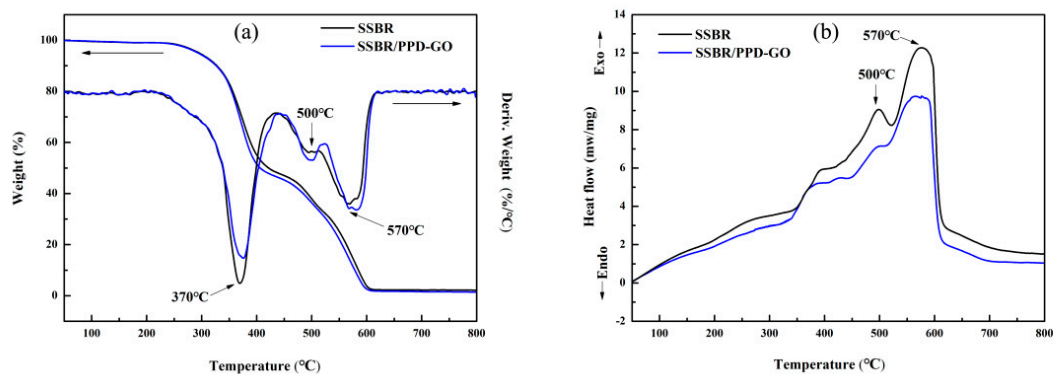


Figure 6. Thermogravimetric-differential scanning calorimeter synchronization analysis (TGA-DSC) curves of SSBR and SSBR/PPD-GO under air atmosphere. (a) The TGA curve; (b) The DSC curve.

3.4. The Micromorphology of SSBR Composites

Variations in the surface morphology of SSBR composites were illustrated by SEM. In Figure 7a, there were obvious pores between GO and the SSBR matrix. In Figure 7b, the PPD-GO was embedded in the fracture surface and maintained a good interaction with the SSBR matrix. It can be attributed to the grafting of PPD, which weakened the agglomeration of GO.

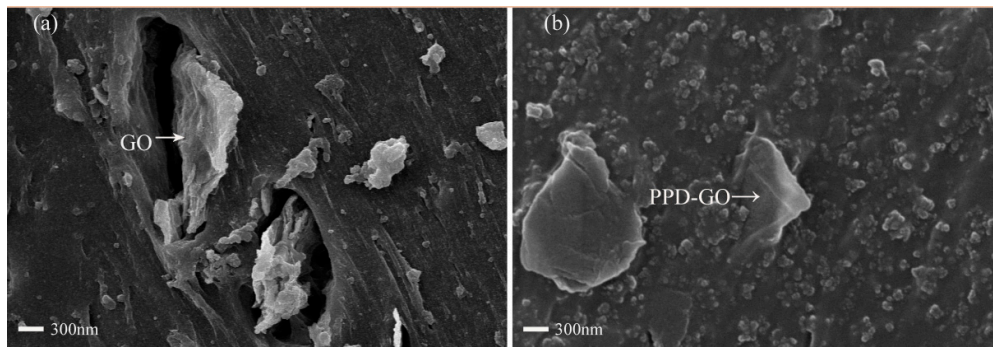


Figure 7. Scanning electron microscopy (SEM) images of fractured surfaces of SSBR/GO (a) and (b) SSBR/PPD-GO4.

3.5. The Dynamic Mechanical Properties of SSBR Composites

It can be seen from Figure 8 that the storage modulus (E') of SSBR/PPD-GO composite was higher than that of the SSBR and the peak in mechanical loss factor ($\tan\delta$) of SSBR/PPD-GO composites moved to high temperature, indicating that the crosslinking density of SSBR/PPD-GO composite was more than that of SSBR. This was due to the strong interaction between PPD-GO and SSBR matrix, which formed many physical crosslink points [41–43].

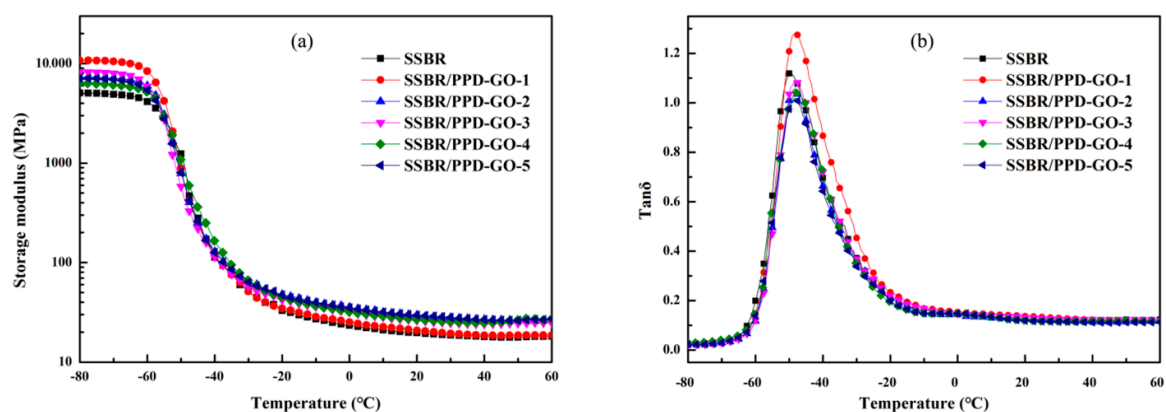


Figure 8. Storage modulus (a) and $\tan\delta$ (b) curves of SSBR composites.

The $\tan\delta$ value at 0 °C and 60 °C was the indicator for evaluation of high performance rubber tire materials [44]. It can be considered that the larger the $\tan\delta$ value at 0 °C, the better wet-skid resistance, and the smaller the $\tan\delta$ value at 60 °C, the less the rolling loss. As shown in Table 4, the $\tan\delta$ value of SSBR/PPD-GO composites at 0 °C was increased. The $\tan\delta$ value of SSBR/PPD-GO1 was 0.153, an increase of 5.5% over that of SSBR. At 60 °C, the $\tan\delta$ value of SSBR/PPD-GO composites was decreased with the content of PPD-GO. The $\tan\delta$ value of SSBR/PPD-GO5 was the smallest, which was 8.9% lower than that of SSBR. This indicated that it had a good effect on improving the wet-skid resistance with the low content of PPD-GO and a positive contribution on reducing the rolling loss with the high content of PPD-GO. Both of wet-skid resistance and low rolling loss of SSBR/PPD-GO4 had been obviously improved, which were 2.1% and 6.5% higher than that of SSBR without PPD-GO.

Table 4. The $\tan\delta$ of SSBR/PPD-GO composites.

Sample	SSBR	PPD-GO1	PPD-GO2	PPD-GO3	PPD-GO4	PPD-GO5
0 °C	0.145	0.153	0.145	0.146	0.148	0.147
	±0.0002	±0.0001	±0.0002	±0.0001	±0.0001	±0.0002
60 °C	0.123	0.119	0.116	0.120	0.115	0.112
	±0.0001	±0.00023	±0.0002	±0.0003	±0.0001	±0.0001

4. Conclusions

In this study, GO grafted by PPD was added into SSBR to give SSBR/PPD-GO composites. The interaction between GO and the SSBR matrix was enhanced by introducing PPD. PPD-GO can be considered the good particle to increase the mechanical properties and aging resistance of SSBR. When the content of PPD-GO was 4 phr, the tensile strength and elongation at break were 21.5 MPa and 350% respectively, which were 29.5% and 16.7% higher than those of SSBR. After aging, the mechanical properties of SSBR/PPD-GO composites were also better than that of SSBR, in which the tensile strength was about 1.3 MPa higher. PPD-GO effectively improved the thermal oxidative aging resistance of SSBR. The better wet-skid resistance and lower rolling loss of SSBR was increased by adjusting the content of PPD-GO. In particular, both of wet-skid resistance and low rolling loss of SSBR/PPD-GO4 had been improved, which were 2.1% and 6.5% higher than that of SSBR respectively. This research can be thought of as an effective method to obtain the SSBR composite with good integrated properties in aging resistance, wet-skid resistance and low rolling loss.

Author Contributions: S.W., X.L. performed the experiments. S.W. wrote the manuscript; H.Z. provided the experimental materials and tested the experimental samples. X.L. conceived and designed the experiments; X.H. contributed to the conception of the study; S.C. (Songbo Chen), S.C. (Shuwei Cai) contributed significantly to the analysis and manuscript preparation; X.H. performed the data analyses; R.Z. contributed significantly to improving the laconics and smoothness of the manuscript. All authors have read and agreed to the published version of the manuscript.

Funding: This research received no external funding.

Acknowledgments: The authors thank the Sichuan University for the supply of DMA used in this study.

Conflicts of Interest: The authors declare no conflict of interest.

References

- Xiao, L.; Zhao, S. Study on structure and properties of SSBR/SiO₂ co-coagulated rubber and SSBR filled with nanosilica composites. *J. Appl. Polym. Sci.* **2008**, *109*, 3900–3907.
- Li, H.; Sun, J.; Song, Y.; Zheng, Q. The mechanical and viscoelastic properties of SSBR vulcanizates filled with organically modified montmorillonite and silica. *J. Mater. Sci.* **2009**, *44*, 1881–1888. [[CrossRef](#)]
- Ge, G.; Sun, A.; Li, S.; Huang, Z. Effect of silane coupling agent Si69 on the hot air aging properties of SSBR/SiO₂ vulcanizates. *World Rubber Ind.* **2013**, *40*, 7–11.
- Luo, K.; Zheng, W.; Zhao, X.; Wang, X.; Wu, S. Effects of antioxidant functionalized silica on reinforcement and anti-aging for solution-polymerized styrene butadiene rubber: Experimental and molecular simulation study. *Mater. Des.* **2018**, *154*, 312–325. [[CrossRef](#)]
- Zhou, S.; Yang, C.; Hu, J.; He, X.; Zhang, R. Damping analysis of some inorganic particles on poly(butyl-methacrylate). *Materials* **2018**, *11*, 992. [[CrossRef](#)]
- Zhong, R.; Zhang, Z.; Zhao, H.; He, X.; Wang, X.; Zhang, R. Improving thermo-oxidative stability of nitrile rubber composites by functional graphene oxide. *Materials* **2018**, *11*, 921. [[CrossRef](#)]
- Tropin, T.V.; Gunnar, S.; Jörn, W.P.S.; Christoph, S. Heat capacity measurements and modeling of polystyrene glass transition in a wide range of cooling rates. *J. Non-Cryst. Solids* **2015**, *409*, 63–75. [[CrossRef](#)]
- Scherillo, G.; Marino, L.; Giovanna, G.B.; Zhan, Y.H.; Xia, H.S.; Giuseppe, M.; Luigi, A. Tailoring assembly of reduced graphene oxide nanosheets to control gas barrier properties of natural rubber nanocomposites. *Acs Appl. Mater. Interfaces* **2014**, *6*, 2230–2234. [[CrossRef](#)]

9. Li, T.; Shi, Z.; He, X.; Jiang, P.; Lu, X.; Zhang, R.; Wang, X. Aging-resistant functionalized lhd-sas/nitrile-butadiene rubber composites: preparation and study of aging kinetics/anti-aging mechanism. *Materials* **2018**, *11*, 836. [[CrossRef](#)]
10. He, X.; Li, T.; Shi, Z.; Wang, X.; Xue, F.; Wu, Z.; Che, Q. Thermal-oxidative aging behavior of nitrile-butadiene rubber/functional LDHs composites. *Polym. Degrad. Stab.* **2016**, *133*, 219–226. [[CrossRef](#)]
11. Chen, Y.; Peng, Z.; Kong, L.; Huang, M.; Li, P. Natural rubber nanocomposite reinforced with nano silica. *Polym. Eng. Sci.* **2008**, *48*, 1674–1677. [[CrossRef](#)]
12. Das, A.; Stöckelhuber, K.W.; Jurk, R.; Saphiannikova, M.; Fritzsche, J.; Lorenz, H.H.; Klüppel, M.; Heinrich, G. Modified and unmodified multiwalled carbon nanotubes in high performance solution-styrene-butadiene and butadiene rubber blends. *Polymer* **2008**, *49*, 5276–5283. [[CrossRef](#)]
13. Yoo, Y.; Cui, L.; Yoon, P.J.; Paul, D.R. Morphology and mechanical properties of rubber toughened amorphous polyamide/mmt nanocomposites. *Macromolecules* **2009**, *43*, 615–624. [[CrossRef](#)]
14. Mishra, S.; Shimpi, N.G.; Mali, A.D. Surface modification of montmorillonite (MMT) using column chromatography technique and its application in silicone rubber nanocomposites. *Macromol. Res.* **2012**, *20*, 44–50. [[CrossRef](#)]
15. Dikin, D.A.; Stankovich, S.; Zimney, E.J.; Piner, R.D.; Dommett, G.H.B.; Evmenenko, G.; Nguyen, S.B.T.; Ruoff, R.S. Preparation and characterization of graphene oxide paper. *Nature* **2007**, *448*, 457–460. [[CrossRef](#)]
16. Chen, D.; Feng, H.; Li, J. Graphene oxide: preparation, functionalization and electrochemical applications. *Chem. Rev.* **2012**, *112*, 6027–6053. [[CrossRef](#)]
17. Zhu, Y.; Murali, S.; Cai, W.; Li, X.; Suk, J.; Potts, J.; Ruoff, R.S. Graphene and graphene oxide: synthesis, properties and applications. *Cheminform* **2010**, *22*, 3906–3924.
18. Mao, Y.; Wen, S.; Chen, Y.; Zhang, F.; Panine, P.; Chan, T.; Zhang, L.; Liang, Y.; Liu, L. High performance graphene oxide based rubber composites. *Sci. Rep.* **2013**, *3*, 2508. [[CrossRef](#)]
19. Li, C.; Feng, C.; Peng, Z.; Gong, W.; Kong, L. Ammonium-assisted green fabrication of graphene/natural rubber latex composite. *Polym. Compos.* **2013**, *34*, 88–95. [[CrossRef](#)]
20. Song, S.H.; Jeong, H.K.; Kang, Y.G. Preparation and characterization of exfoliated graphite and its styrene butadiene rubber nanocomposites. *J. Ind. Eng. Chem.* **2010**, *16*, 1059–1065. [[CrossRef](#)]
21. Li, D.; Müller, M.B.; Gilje, S.; Kaner, R.B.; Wallace, G.G. Processable aqueous dispersions of graphene nanosheets. *Nat. Nanotechnol.* **2008**, *3*, 101–105. [[CrossRef](#)] [[PubMed](#)]
22. Stankovich, S.; Piner, R.D.; Nguyen, S.; Ruoff, R. Synthesis and exfoliation of isocyanate-treated graphene oxide nanoplatelets. *Carbon* **2006**, *44*, 3342–3347. [[CrossRef](#)]
23. Niyogi, S.; Bekyarova, E.; Itkis, M.; McWilliams, J.; Hamon, M.; Haddon, R. Solution Properties of Graphite and Graphene. *J. Am. Chem. Soc.* **2006**, *128*, 7720–7721. [[CrossRef](#)] [[PubMed](#)]
24. Liu, Y.; Zhou, J.; Zhang, X.; Liu, Z.; Wan, X.; Tain, J.; Wang, T.; Chen, Y. Synthesis, characterization and optical limiting property of covalently oligothiophene-functionalized graphene material. *Carbon* **2009**, *47*, 3113–3121. [[CrossRef](#)]
25. Tang, Z.; Kang, H.; Shen, Z.; Guo, B.; Zhang, L.; Jia, D. Grafting of polyester onto graphene for electrically and thermally conductive composites. *Macromolecules* **2012**, *45*, 3444–3451. [[CrossRef](#)]
26. Veca, L.M.; Lu, F.; Mezziani, M.; Cao, L.; Zhang, P.; Qi, G.; Qu, L.; Shrestha, M.; Sun, Y. Polymer functionalization and solubilization of carbon nanosheets. *Chem. Commun.* **2009**, *18*, 2565–2567. [[CrossRef](#)]
27. Liu, X.; Kuang, W.; Guo, B. Preparation of rubber/graphene oxide composites with in-situ interfacial design. *Polymer* **2015**, *56*, 553–562. [[CrossRef](#)]
28. Ma, H.L.; Zhang, H.; Hu, Q.; Li, W.; Jiang, Z.; Yu, Z.; Dasari, A. Functionalization and reduction of graphene oxide with p-phenylene diamine for electrically conductive and thermally stable polystyrene composites. *ACS Appl. Mater. Interfaces* **2012**, *4*, 1948–1953. [[CrossRef](#)]
29. Caliman, C.C.; Mesquita, A.; Cipriano, D.; Freitas, J.; Cotta, A.; Macedo, W.; Porto, A. One-pot synthesis of amine-functionalized graphene oxide by microwave-assisted reactions: An outstanding alternative for supporting materials in supercapacitors. *Rsc Adv.* **2018**, *8*, 6136–6145. [[CrossRef](#)]
30. Zhou, J.; Wei, L.; Zheng, J.; Huang, G. The synthesis of graphene-based antioxidants to promote anti-thermal properties of styrene-butadiene rubber. *Rsc Adv.* **2017**, *7*, 53596–53603. [[CrossRef](#)]
31. Zhong, B.; Dong, H.; Luo, Y.; Zhang, D.; Zhang, D.; Jia, Z.; Jia, Z.; Jia, D.; Liu, F. Simultaneous reduction and functionalization of graphene oxide via antioxidant for highly aging resistant and thermal conductive elastomer composites. *Compos. Sci. Technol.* **2017**, *151*, 156–163. [[CrossRef](#)]

32. Li, G.Y.; Koenig, J. FTIR imaging of oxidation of polyisoprene. 2. The role of N-phenyl-N'-dimethyl-butyl-p-phenylenediamine antioxidant. *Polym. Degrad. Stab.* **2003**, *81*, 377–385. [[CrossRef](#)]
33. Hashim, A.S.; Kohjiya, S. Curing of epoxidized natural rubber with p-phenylenediamine. *J. Polym. Sci. Pol. Chem.* **1994**, *32*, 1149–1157. [[CrossRef](#)]
34. Hu, Y.; Shen, J.; Li, N.; Shi, M.; Ma, H.; Yan, B.; Wang, W.; Huang, W.; Ye, M. Amino-functionalization of graphene sheets and the fabrication of their nanocomposites. *Polym. Compos.* **2010**, *31*, 1987–1994. [[CrossRef](#)]
35. Hung, W.S.; Tsou, C.; Guzman, M.; An, Q.; Liu, L.; Zhang, M.; Hu, C.C.; Lee, K.R.; Lai, J.Y. Cross-linking with diamine monomers to prepare composite graphene oxide-framework membranes with varying spacing. *Chem. Mater.* **2014**, *26*, 2983–2990. [[CrossRef](#)]
36. Hussein, A.; Sarkar, S.; Oh, D.; Lee, K.; Kim, B. Epoxy/p-phenylenediamine functionalized graphene oxide composites and evaluation of their fracture toughness and tensile properties. *J. Appl. Polym. Sci.* **2016**, *133*, 34. [[CrossRef](#)]
37. Li, B.; Zhou, L.; Wu, D.; Peng, H.; Yan, K.; Zhou, Y.; Liu, Z. Photochemical chlorination of graphene. *ACS Nano* **2011**, *5*, 5957–5961. [[CrossRef](#)]
38. Wang, Y.; Yu, Y.; Hu, X.; Feng, A.; Jiang, F.; Song, L. p-Phenylenediamine strengthened graphene oxide for the fabrication of superhydrophobic surface. *Mater. Des.* **2017**, *127*, 22–29. [[CrossRef](#)]
39. Song, Y.D.; Gao, Y.; Rong, H.; Wen, H.; Sha, Y.; Zhang, H.; Liu, H.; Liu, Q. Functionalization of graphene oxide with naphthalenediimide diamine for high-performance cathode materials of lithium-ion batteries. *Sustain. Energy Fuels* **2013**, *2*, 803–810.
40. Liao, R.; Tang, Z.; Lei, Y.; Guo, B. Polyphenol-reduced graphene oxide: mechanism and derivatization. *J. Phys. Chem. C* **2011**, *115*, 20740–20746. [[CrossRef](#)]
41. Rui, Z.; He, X.; Lai, Z.; Yang, D. Effect of some inorganic particles on the softening dispersion of the dynamics of butyl rubber. *Polym. Bull.* **2016**, *74*, 1–13.
42. Zhang, R.; He, X.; Yu, H. Why $\tan\delta$ of poly (butyl acrylate) and poly (ethyl acrylate) with little double bonds are becoming asymmetric? *Polymer* **2014**, *55*, 4720–4727. [[CrossRef](#)]
43. Zhang, R.; He, X.; Rodrigues, A.; Guo, Q. Softening dynamics of polymer blends and composites investigated by differential spectra of dynamic mechanical analysis. *Adv. Polym. Technol.* **2017**, *37*, 2504–2509. [[CrossRef](#)]
44. Lin, Y.; Liu, S.; Peng, J.; Liu, L. The filler–rubber interface and reinforcement in styrene butadiene rubber composites with graphene/silica hybrids: A quantitative correlation with the constrained region. *Compos. Part A Appl. Sci. Manuf.* **2016**, *86*, 19–30. [[CrossRef](#)]



© 2020 by the authors. Licensee MDPI, Basel, Switzerland. This article is an open access article distributed under the terms and conditions of the Creative Commons Attribution (CC BY) license (<http://creativecommons.org/licenses/by/4.0/>).